Received: 8 May 2024 | Revised: 12 July 2024 | Accepted: 11 August 2024

DOI: 10.1111/ijac.14916

International Journal of Applied Ceramic Technology

RESEARCH ARTICLE

Synthesis and characterization of the doped/co-doped SnO_2 nanoparticles by the sol–gel method

Fatma Aydın Ünal

Department of Metallurgy and Materials Engineering, Alanya Alaaddin Keykubat University, Antalya, Turkey

Correspondence
Fatma Aydın Ünal, Department of Metallurgy and Materials Engineering, Alanya Alaaddin Keykubat University, Antalya 07425, Turkey.
Email: fatma.aydin@alanya.edu.tr

Abstract

Tin oxide (SnO_2) is one of the important semiconductors used in the application of solar cells because of its chemical–mechanical stability and wide band gap. These properties are very important for the performance development and photoanode optimization of a dye-sensitized solar cell (DSSC). However, the low conduction band value of SnO_2 reduces the photovoltaic efficiency, which limits the application of DSSC. Therefore, the doping strategy was used to increase the sensitivity to the visible light spectrum and change the light absorption properties of SnO_2. In this paper, pure SnO_2, Ag/SnO_2, Pt/SnO_2, and $Pt/Ag/SnO_2$ nanoparticles were synthesized at the nanoscale by a simple chemical sol–gel method. To characterize the structure, morphological/chemical properties, optical properties, and surface properties of the synthesized SnO_2 nanoparticles, X-Ray Diffraction (XRD), ultraviolet–visible, Brunauer–Emmett–Teller, Scanning Electron Microscopy (SEM)/Energy Dispersive X-Ray Spectroscopy (EDX), Transmission Electron Microscopy (TEM), and particle size analysis were respectively used. XRD results showed that the crystal sizes varied between 8.8 and 12.2 nm depending on the doping. Doping processes resulted in reductions in particle sizes. Optical studies resulted in decreases in the band gap with the doping process. The conclusions obtained have shown that Ag doping, and Pt–Ag co-doping can be promising for use as photoanode materials in semiconductor technology and especially in DSSC applications.

KEYWORDS
characterization, SnO2, solar cell, sol–gel, synthesis

1 | INTRODUCTION

One of the most common application areas of semiconductor oxides is dye-sensitized solar cell (DSSC) technology.[1–3] DSSCs have interested researchers and industries due to their low manufacturing costs, high power conversion efficiency, easy and environmentally friendly fabrication process, and good optical and electrochemical properties.[4–6] Despite all this, their productivity, stability, and industrial production still need to increase. SnO_2 photoelectrode, new organic photosensitizers, and new electrolytes, for efficient catalyst materials encompass diverse changes

that have emerged within DSSC recently.[5] The basic constituents of a typical DSSC are a dye-anchored mesoporous photoanode, an electrolyte, and a counter electrode.[5,6] Among these components, the photoanode material plays a significant role in improving the performance of DSSCs.[7] The photoanode is liable for providing active sites for dye adsorption and the proper transport mechanism of photo-generated electrons.[8] To achieve high-performance DSSC, photoanodes are required to have a large surface area, high electron transfer efficiency, and low electron recombination. Tin oxide (SnO_2), one of the DSSC photoanodes, is used as an alternative semiconductor oxide to conventional photoanodes.[5] SnO_2 has an optical (direct) transition corresponding to ~3.6 eV due to its n-type semiconductor crystal structure. Compared to other photoelectrode materials, a wide band gap, higher electron mobility, and low sensitivity to UV make SnO_2 more stable for a long time, making it promising for photoanode materials.[5,9] This indicates faster transport of photogenerated electrons and longer-term stability of the electrons. However, the conduction band value of SnO_2 is relatively low. Its photovoltaic efficiency is low due to inadequate dye adsorption and the low energy value of the conduction band, which restricts its practice in DSSCs. Although it is advantageous in many ways, it has some disadvantages such as wide band gap and increased charge carrier recombination. However, recently these problems have begun to attract considerable attention in the literature. Researchers have used many strategies to modify the light absorption properties of SnO_2 to extend its sensitivity to the visible light spectrum. A particularly effective way includes metal doping. Significant changes can be observed in the optical and electrical properties of SnO_2 after doping with anionic and cationic dopants. The incorporation of cationic dopants into SnO_2 can cause the formation of new electronic bands or changes in electronic energy levels by overlapping bands, and these alterations can develop the photoresponse in the visible region.[8,10] To change the band gap of the photoanode, doping efforts with suitable metal that can modulate the optical properties of the photoanode have been studied in the literature.[11–15] Panneer et al. synthesized aluminum (Al) doped tin oxide nanoparticles, containing different concentrations (.5, 1, and 5 mol) of Al. X-Ray Diffraction (XRD) results showed the uniform crystal structure of the samples prepared for Al-doped SnO_2 nanoparticles, Field Emission Scanning Electron Microscopy (FESEM) analysis revealed that the particle size was narrowed during doping with Al, and the optical and surface characteristics of SnO_2 nanoparticles increased significantly.[16] Khan et al. obtained Ni-doped SnO_2 nanoparticles at different nickel concentrations by the sol–gel method. They examined transmittance, particle size variation, band gap, and optical properties. It was been reported that doping did not affect morphologies and structures while changing the particle size and reducing the band gap.[17] Lachore et al. synthesized undoped SnO_2, Cu-doped and (Ni, Cu) co-doped SnO_2 nanoparticles via the sol–gel method. The XRD study supported that the prepared samples had the tetragonal rutile crystal structure for all mono-doped/co-doped and undoped SnO_2 nanoparticles. By ultraviolet–visible (UV–vis) diffusion reflection spectroscopy analysis, it was declared that the optical band gap reduced from 3.38 to 3.27 eV when dopant concentrations were raised.[18]

As an alternative to SnO_2, semiconductor materials such as TiO_2, ZnO, and $BaSnO_3$ are also used as photoanodes in DSSC.[5] Dhonde et al. synthesized pure and copper/nitrogen (Cu/N) doped TiO_2 nanoparticles via the sol–gel method. The results showed that adding appropriate amounts of Cu and N ingredients to TiO_2 could change its optical and electrical properties by increasing the absorption in the visible region and decreasing the band gap. It was also mentioned that adding a sufficient amount of Cu/N to TiO_2 could cause smaller particle size, higher specific surface area, enhanced dye adsorption, and delayed charge carrier recombination.[19] Mahajan et al. synthesized pure and Zn-doped $BaSnO_3$ micro rods with varying doping concentrations. Structural analysis verified the presence of a pure body-centered cubic phase in barium stannate, while morphological investigation disclosed the formation of micro rods accompanied by surface particle aggregation. Optical examination showed an important reduction in reflection intensity and band gap values with growing Zn concentration.[20] Ünal et al. synthesized undoped ZnO and 5 wt% Gd/K co-doped ZnO compounds at the nanoscale to increase photocatalytic activity. In their photocatalytic activity test results, it was reported that Gd/K-doped ZnO showed ~66% degradation in 60 min, while undoped ZnO showed ~52% degradation at the same time.[21]

Among various methods, the sol–gel method has advantages such as being easily reproducible, using simple laboratory equipment (does not require any high-tech equipment), having a low impurity rate, taking less time, being low-cost, and being easy to process.[9,22]

Pure SnO_2 cannot be excited by visible light due to its wide band gap of ~3.6 eV. Therefore, doping processes aim to narrow the band gap of SnO_2 and increase light absorption.[23] In this paper, the effect of doping was examined by investigating the use of synthesized SnO_2 nanoparticles as photoanode material. Thus, it was aimed to enlight the effect of Ag and Pt doping on the structural, morphological, and optical properties of SnO_2, and targeted a significant contribution to the literature by revealing the complex interaction between the dopant and the host matrix. The doping strategy was used to prepare Ag/Pt-doped and Pt–Ag co-doped SnO_2 as photoanode, while the sol–gel technique was chosen for

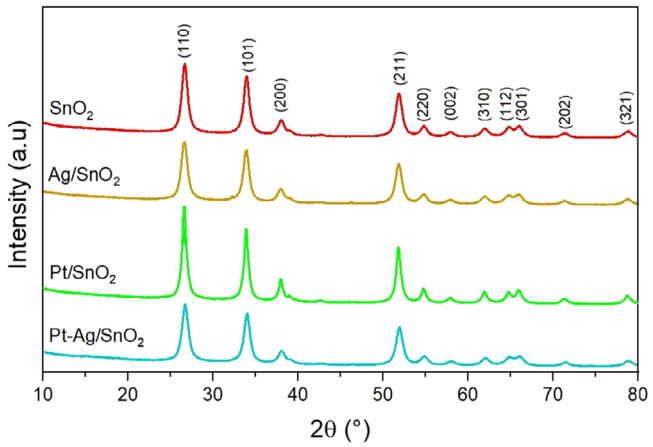

FIGURE 1 XRD graph of the SnO_2 samples.

the synthesis of SnO_2 nanoparticles due to the above-mentioned advantages. The structures, morphological/chemical compositions, optical properties, and surface characteristics of the obtained nanoparticles were investigated.

2 | METHODS

2.1 | Materials

Tin(II) chloride ($SnCl_2$) was supplied from Sigma–Aldrich having a molecular weight of 189.62 (≥99.99% pure). Platinum(IV) chloride ($PtCl_4$) was supplied from Sigma–Aldrich having a molecular weight of 336.89 (≥99.99% pure). Silver chloride (AgCl) was supplied from Sigma–Aldrich having a molecular weight of 143.32. Citric acid monohydrate was supplied from Sigma–Aldrich having a molecular weight of 210.14 (≥98% pure). 2-Propanol was purchased from Sigma–Aldrich. Distilled water was used as the solvent.

2.2 | Synthesis

2.2.1 | SnO_2 synthesis

To obtain SnO_2 nanoparticles, precursor solutions were prepared using the sol–gel method. To prepare a .25 M, 100 mL $SnCl_2$ solution, 5.64 g of $SnCl_2$ was weighed, and then propanol-2 was added up to the volume line of the 100 mL volumetric flask. The $SnCl_2$ solution taken into the beaker was continuously mixed in a magnetic stirrer for 30 min. Thus, 100 mL of $SnCl_2$ solution was prepared. Then, a propanol-2 solution of citric acid monohydrate was prepared. 100 mL of .25 M citric acid monohydrate solution was added dropwise into the $SnCl_2$ solution and allowed to mix for another 30 min. The temperature was fixed at 80°C. It was allowed to mix in this way for approximately 90 min. At the end of this period, when the necessary evaporation processes were completed, the SnO_2 mixture turned into a gel. The resulting gel was allowed to dry in the furnace at 120°C for 20 h. The dried gel was calcined in the oven at 450°C for 150 min and turned into powder.

2.2.2 | Doped SnO_2 synthesis

Pt-doped SnO_2 nanoparticles were synthesized by the sol–gel technique. .25 M $SnCl_2$-containing 50 mL of propanol-2 solution (A) was prepared. .0025 M, .042 g Pt(IV) chloride-containing 50 mL of solution (B) was prepared in a separate volumetric flask. .25 M citric acid monohydrate-containing 100 mL of propanol-2 solution (C) was prepared in another volumetric flask. Solution B was added dropwise to the obtained solution A, and then mixed in a magnetic stirrer for 30 min. The temperature was gradually increased from room temperature to 80°C. Then, solution C was added dropwise to the obtained solution. The temperature was fixed at 80°C and mixing was continued until the final mixture turned into a gel. The oven and furnace process for pure SnO_2 was repeated. A similar process was applied for Ag-doped SnO_2.

2.2.3 | Co-doped SnO_2 synthesis

Pt and Ag co-doped SnO_2 nanoparticles were synthesized by the sol–gel technique. .25 M, 5.64 g $SnCl_2$-containing 50 mL of propanol-2 solution (A) was prepared. .25 M citric acid monohydrate-containing 100 mL of propanol-2 solution was prepared in a separate volumetric flask. .0025 M, .042 g Pt(IV) chloride-containing 50 mL propanol-2 solution (B) was prepared in another volumetric flask. .0025 M, .0179 g silver chloride (AgCl)-containing 50 mL propanol-2 solution (C) was prepared in another volumetric flask. B and C solutions were added dropwise to solution A and mixed for 30 min on a magnetic stirrer. Then, the temperature was gradually increased. Meanwhile, the citric acid solution was joined dropwise to the resulting final solution and mixing was continued. The temperature was fixed at 80°C and mixing was continued on the magnetic stirrer until the final mixture became a gel. Drying and baking steps were performed in the same way as for pure SnO_2.

2.3 | Characterization

XRD diffractometer (PANalytical Empyrean) with a Cu Kα1 (λ = 1.54059 Å) radiation source was used to elucidate the structures of the powders. Morphological

TABLE 1 XRD parameters of the SnO_2 nanoparticles.

Samples	Planes (*h k l*)	2θ (deg)	FWHM (deg)	Dislocation density (δ) (lines m^{-2})	Crystallite size (nm)	Microstrain (ε)
SnO_2	1 1 0	26.66	.97152	.012980558	8.777146	.017888
	1 0 1	33.94	.88917	.010505446	9.756471	.012713
	2 1 1	51.87	.88962	.009296001	10.37175	.00798
Ag/SnO_2	1 1 0	26.62	1.04237	.014945379	8.179873	.018162
	1 0 1	33.90	.92846	.011456911	9.342567	.01616
	2 1 1	51.85	.91497	.009835557	10.08325	.015867
Pt/SnO_2	1 1 0	2.61	.7035	.006807823	12.11981199	.012978
	1 0 1	33.90	.73739	.00722647	11.76350886	.010555
	2 1 1	51.83	.71184	.005954075	12.9596373	.006392
$Pt–Ag/SnO_2$	1 1 0	26.65	1.023	.017097	7.987682463	.019676
	1 0 1	33.95	1.023	.013681	8.932871302	.013897
	2 1 1	51.89	1.023	.011551	9.72163306	.008516

Abbreviation: FWHM, Full width at half maximum.

TABLE 2 Summary of structural properties of the pure SnO_2, Pt-doped, Ag-doped, and Pt and Ag co-doped SnO_2 nanoparticles.

Samples	Average crystallite size (nm)	Average microstrain (ε)	Average dislocation density (δ) (lines m^{-2})
SnO_2	9.635121	.01286	.010927
$Ag–SnO_2$	9.201897	.01673	.012079
$Pt–SnO_2$	12.28099	.009975	.006663
$Pt–Ag/SnO_2$	8.880729	.01403	.01411

and chemical properties of SnO_2 powders synthesized at the nanoscale were examined by SEM/EDX (Scanning Electron Microscopy/Energy Dispersive X-Ray Spectroscopy, Zeiss Sigma 300) and TEM (Transmission Electron Microscopy, JEOL JEM-1400 Plus) analyses. The UV–vis absorption characteristic of sample nanoparticles was made by a UV–vis spectrophotometer (Shimadzu UV-3600 Plus). The Brunauer–Emmett–Teller (BET) surface area of nanoparticles was obtained by a surface area analyzer (Micromeritics 3Flex). The particle size characteristics of SnO_2 nanoparticles were made by a particle size analysis (Malvern Zetasizer Nano ZSP).

3 | RESULTS

3.1 | Structure properties

3.1.1 | XRD analysis

To characterize the crystalline structures and crystallite size of the synthesized doped SnO_2 nanoparticles, XRD analysis was done using a Cu-Kα source (with a 2θ range of 20°–90°, a scanning speed of 2° min^{-1}, a voltage of 45 kV, and a current of 40 mA). The obtained XRD pattern of SnO_2, Ag/SnO_2, Pt/SnO_2, and, $Pt-Ag/SnO_2$ is shown in Figure 1. The prominent diffraction peaks at 26.58°, 33.86°, 38.1°, 51.76°, and 64.7° are determined to (1 1 0), (1 0 1), (2 0 0), (2 1 1), (2 2 0), (3 1 0), (1 1 2), (3 0 1), (2 0 2), and (3 2 1) diffraction planes of the SnO_2 crystal structure, respectively. These consequences are in agreement with the tetragonal (rutile) crystal phase of SnO_2 nanoparticles.[24,25] According to the XRD pattern, it can be seen that there is no peak shift in the pattern of synthesized SnO_2 when compared to pure SnO_2. This indicates that pure and doped SnO_2 was successfully synthesized using the sol–gel method. This result is in agreement with the literature. It was reported by Setiadji et al. that there has been no peak shift in the XRD pattern of synthesized SnO_2. It has been stated that the crystal structure of the synthesized SnO_2 has a tetragonal crystal structure, which is the structure of the SnO_2 standard. Therefore, it has been declared that SnO_2 was successfully synthesized by the hydrothermal method.[26]

It is seen that there are some small peaks in all of the samples representing various miller indices of the tetragonal phase of SnO_2 and the obtained XRD pattern is compatible with the literature.[27] The lack of extra peaks above the standard peaks verifies that the synthesized SnO_2 nanoparticles are single-phase and do not embody any impurities.[24]

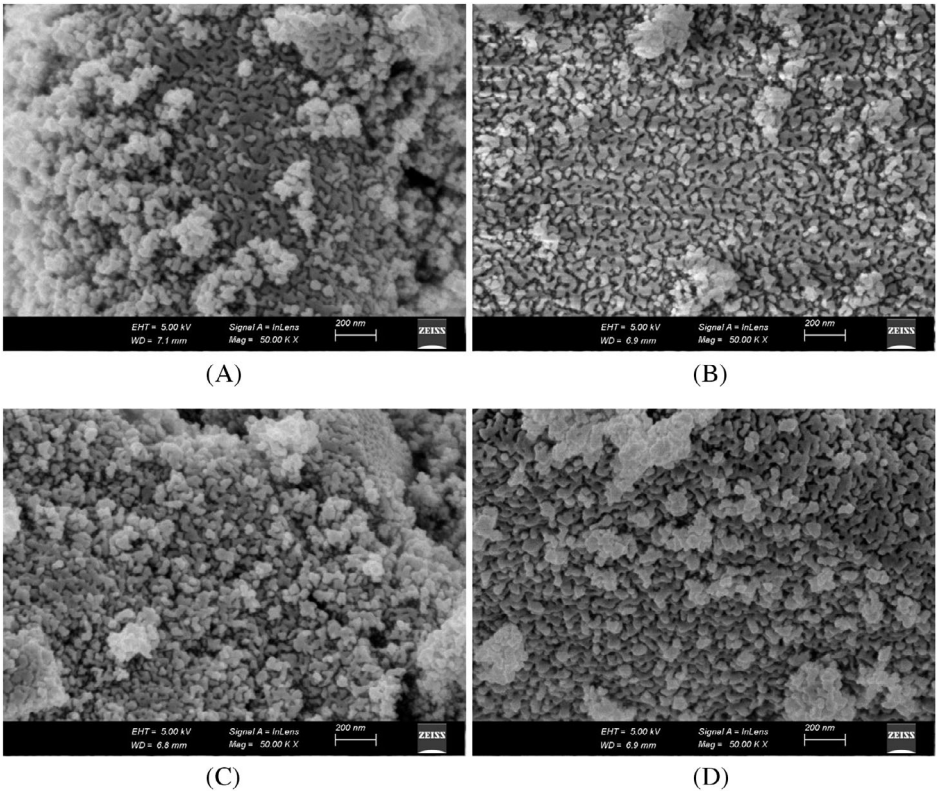

FIGURE 2 SEM images of synthesized (A) SnO_2, (B) Pt/SnO_2, (C) Ag/SnO_2, and (D) Pt–Ag/SnO_2.

Grain sizes, dislocation densities, and microstrain values of the SnO_2 nanoparticles were calculated using XRD pattern data. The crystal size of the SnO_2 samples examined by the XRD method was determined with the help of the Debye–Scherrer equation given in Equation (1):

$$L = k\lambda/\beta \cos\theta, \tag{1}$$

where "L" symbolizes crystallite size, "K" is the shape factor having a value of .9, λ is the wavelength of the applied X-rays a constant value (1.54059 Å), "β" demonstrates full-width at half-maximum of the peak, and θ is the Bragg angle at which the plane is observed.[28] The crystallite sizes of SnO_2 samples were computed with the help of Equation (1).

$$\varepsilon = \beta/4\tan\theta. \tag{2}$$

Microstrain (ε) values were calculated from Equation (2).

$$\delta = 1/L^2 \tag{3}$$

Information about crystallization levels can be obtained by looking at the dislocation density (δ) value, which offers the length of dislocation lines per unit volume of the crystal. Since dislocation in the crystal structure affects the morphological feature of the material, the formation of particles, and particle size, dislocation densities (δ) were computed using the Williamson–Smallman relationship.[29,30] Dislocation densities (δ) were computed with the formula given in Equation (3).

The XRD parameters obtained for prominent (1 1 0), (1 0 1), and (2 1 1) planes of synthesized SnO_2 nanoparticles are given in Table 1.

Table 2 summarizes the average values of the parameters of SnO_2 nanoparticles. While Pt doping increased the average crystal size, Ag and Pt–Ag doping decreased the average crystal size. Especially in co-doping (Pt–Ag/SnO_2) the lowest average crystal size was obtained. A coherent narrowing of the peaks of the Pt-doped sample was observed (Figure 1). This narrowing reflects a reduction in full width at half maximum (FWHM). This narrowing of the peaks is attributed to the increment in the average crystallite size of the nanoparticles.[24,31] Therefore, the average crystallite size of the Pt-doped SnO_2 was obtained higher than other SnO_2 samples. While the average microstrain values decreased with Pt doping, they increased with Ag and Pt–Ag doping. It was concluded that the average dislocation density diminished with Pt doping and increased with Ag and Pt–Ag doping. A small dislocation density value indicated that the crystallization level was good.[32,33] It was observed that the crystallite size, dislocation density, and microstrain values calculated in this study were compatible with the literature.[34]

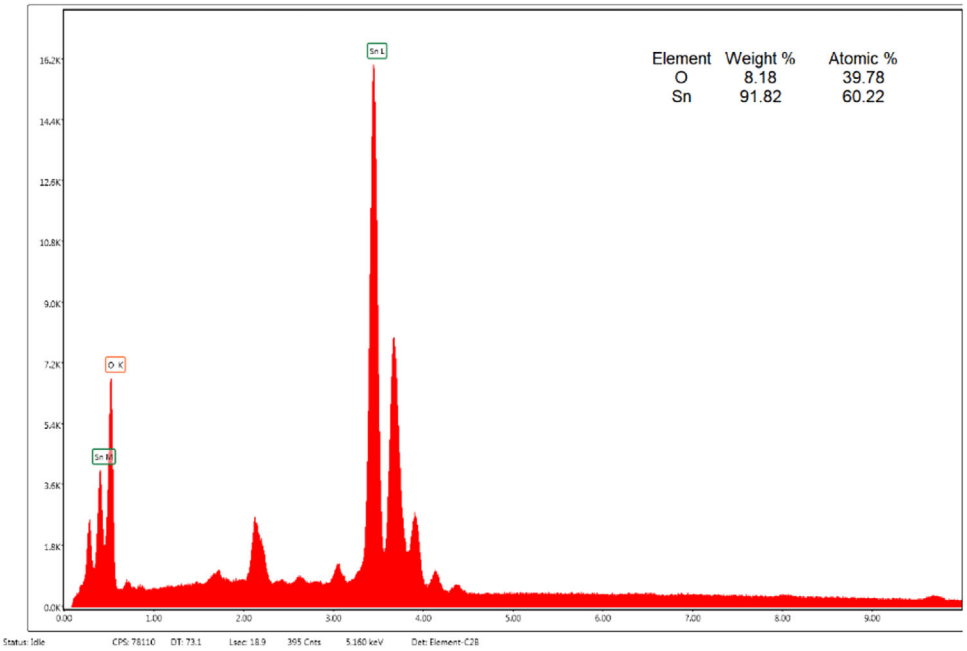

(A)

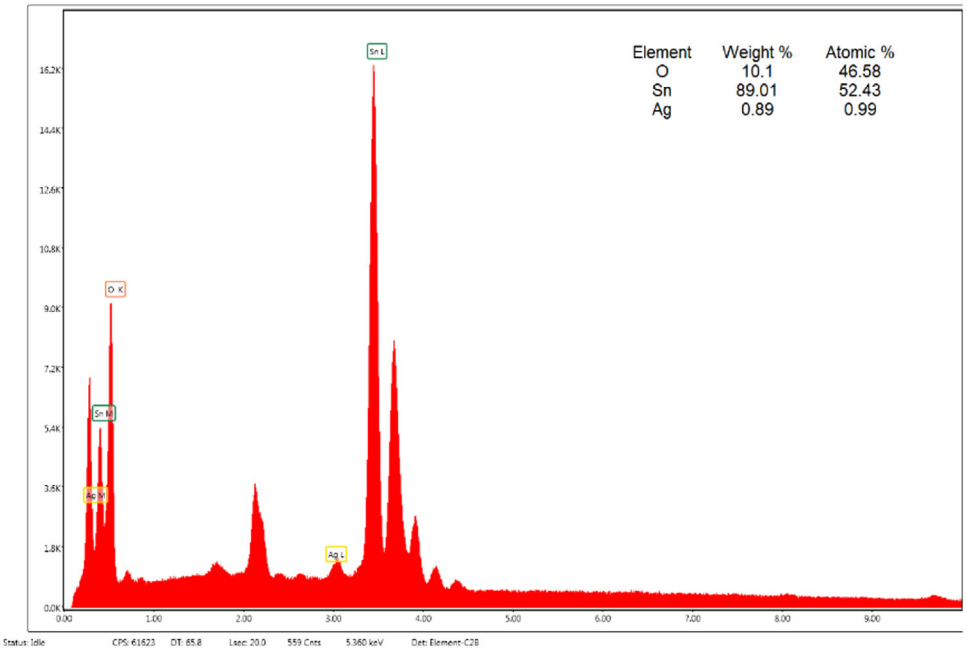

(B)

FIGURE 3 EDX analysis of synthesized (A) SnO_2, (B) Ag/SnO_2, (C) Pt/SnO_2, and (D) $Pt–Ag/SnO_2$.

3.2 | Morphological and chemical properties

3.2.1 | SEM/EDX analysis

The morphological properties of the synthesized SnO_2 samples were investigated with the Scanning Electron Microscopy (SEM) image given in Figure 2A–D. From the images obtained, it is clear that the pure SnO_2 sample (Figure 2A) has rod-like structures and agglomerates. While the morphological properties almost did not change with Pt doping (Figure 2B), the rod-like structure tended to have slightly circular-shaped particles with Pt–Ag (Figure 2C) and especially Ag doping (Figure 2D). Moreover, the homogeneity in the structure and agglomerations tended to rise with Ag and Pt–Ag doping. Since

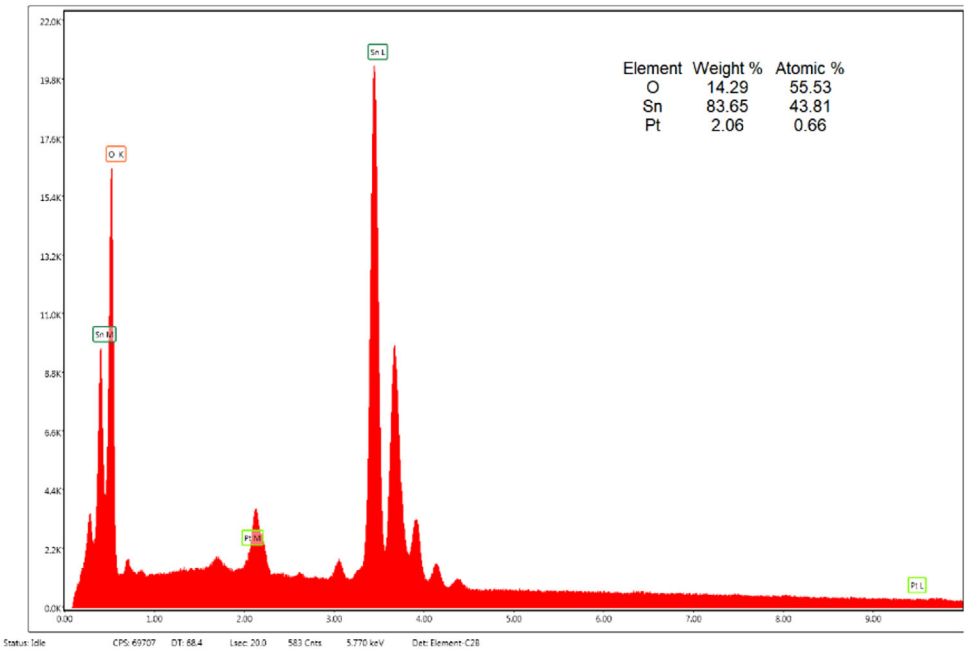

(C)

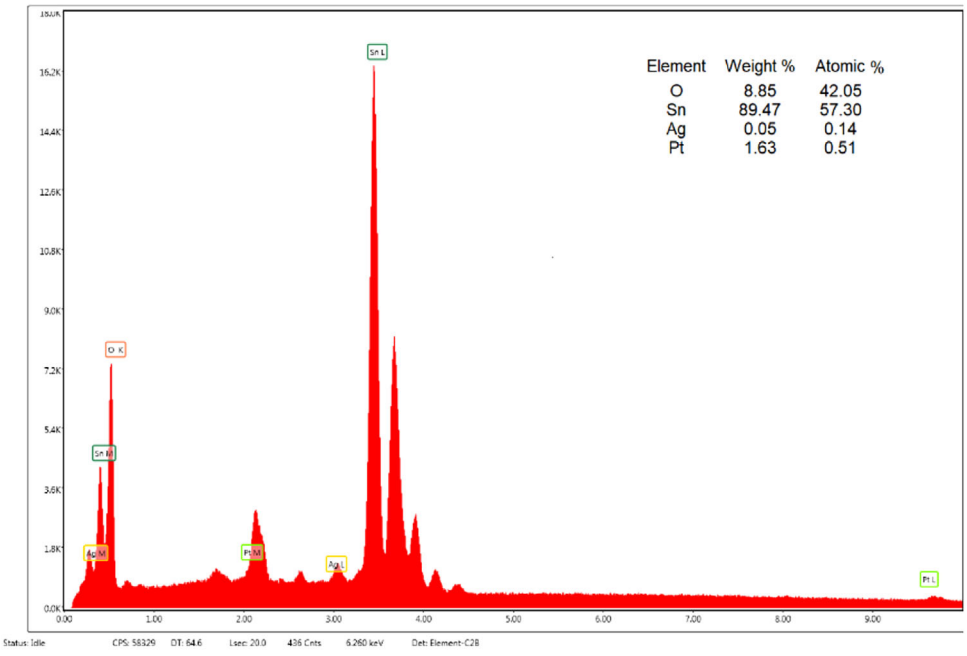

(D)

FIGURE 3 Continued

Ag and Pt/Ag doping has less tendency to agglomerate than pure SnO_2 and Pt doping, it was observed by SEM analysis that the average particle size decreased further with Ag and Pt/Ag doping, and this was confirmed by XRD analysis and nanoparticle size obtained from BET analysis. Guo et al. synthesized Ag-doped SnO_2 nanoparticles hydrothermally. The morphology and microstructure of Ag/SnO_2 were examined by the SEM. It was stated that the prepared films showed agglomeration with an irregular morphology. Additionally, it was been shown via SEM images that the samples consist of irregularly shaped sphere-like structures. It has been reported that the morphology of Ag-doped SnO_2 samples is similar to the pure SnO_2 morphology even with different Ag doping amounts.[35]

The Energy Dispersive X-Ray Spectroscopy (EDX) system added to the SEM device was used to evaluate the elemental composition of the samples. Figure 3A–D shows

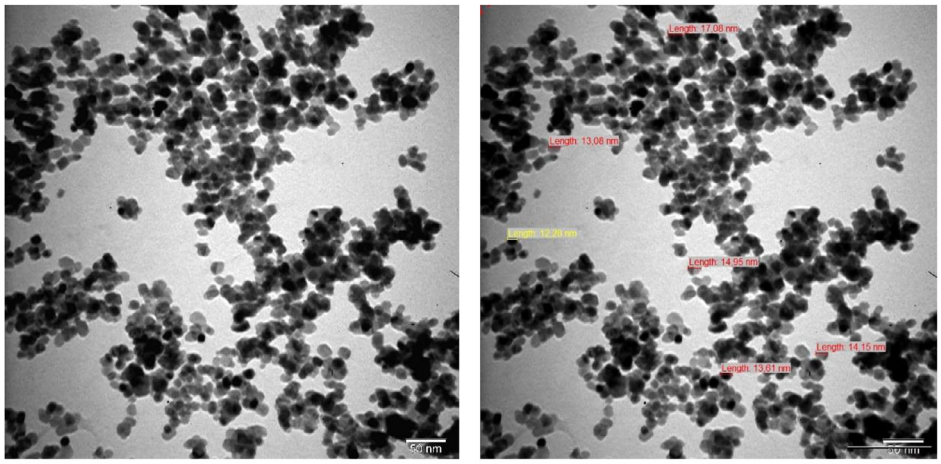

(A)

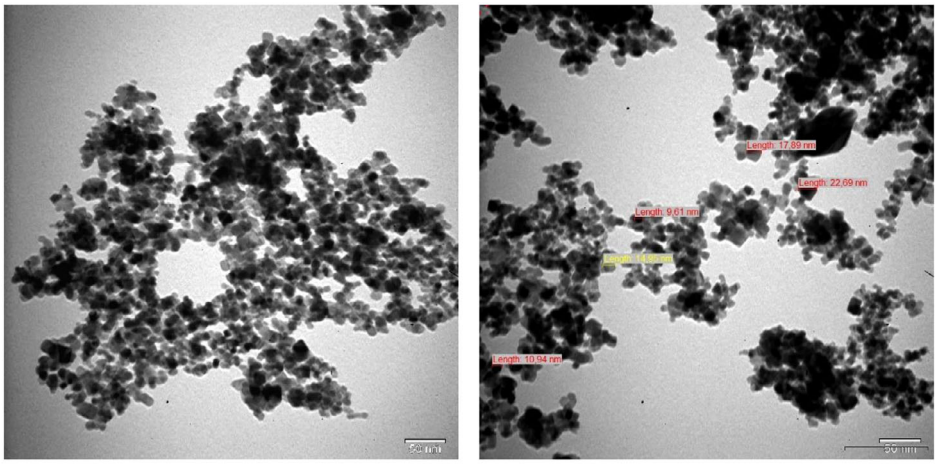

(B)

FIGURE 4 TEM images of (A) pure SnO_2, (B) Pt/SnO_2, (C) Ag/SnO_2, and (D) Pt–Ag/SnO_2 nanoparticles.

the weight% and atomic% of the elements corresponding to the synthesized SnO_2 samples. In the analysis, it was observed that Sn and O peaks were mostly available in suitable proportions. This confirmed the presence of SnO_2 samples. At the same time, the presence of Ag, Pt, and Pt–Ag doping in the analysis showed that the doping process was successful.

3.2.2 | TEM analysis

To better explain the shape and size of particles in the synthesized SnO_2 samples, TEM images were investigated. The TEM images of pure SnO_2, Pt/SnO_2, Ag/SnO_2, and Pt–Ag/SnO_2 nanoparticles are shown in Figure 4A–D, respectively. All the synthesized nanoparticles showed highly aggregated structures because of small particle sizes.[6] It can be observed from TEM images that both pure and doped/co-doped SnO_2 nanoparticles led to aggregation as particle size was smaller. The SnO_2 nanoparticles have partially irregularly shaped particles with a size ranging from 8 to 20 nm. The obtained TEM results confirm the SEM images and particle size analyses. Sery et al. TEM images of SnO_2-based samples synthesized using sol–gel and sonochemical methods and then calcined at 250°C, 500°C, and 750°C were examined. An increase in particle size was observed with increasing calcination temperature. It has been reported that based on the surface area and TEM particle size values, tin oxides calcined at 250°C were expected to show higher photocatalytic activity in among all samples and were selected for further photocatalytic experiments.[36]

3.3 | Physical properties

3.3.1 | BET analysis

For the synthesized SnO_2 samples, nitrogen adsorption–desorption measurements were performed to get

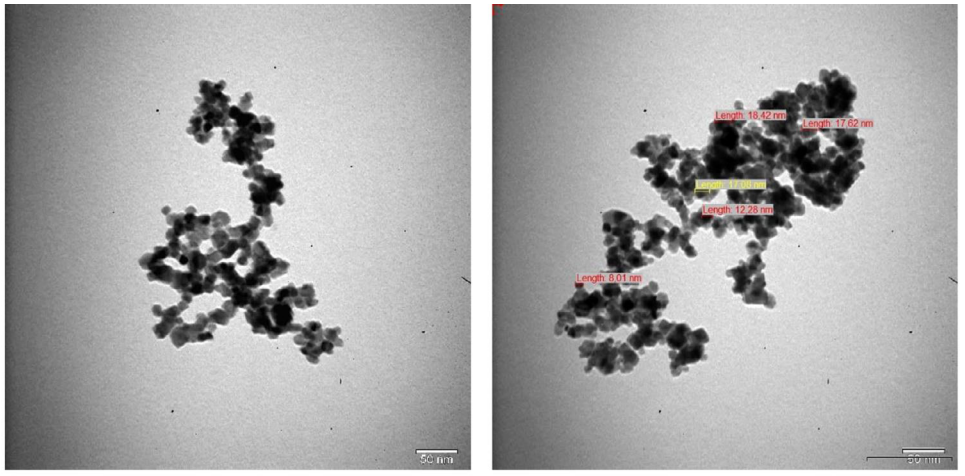

(A)

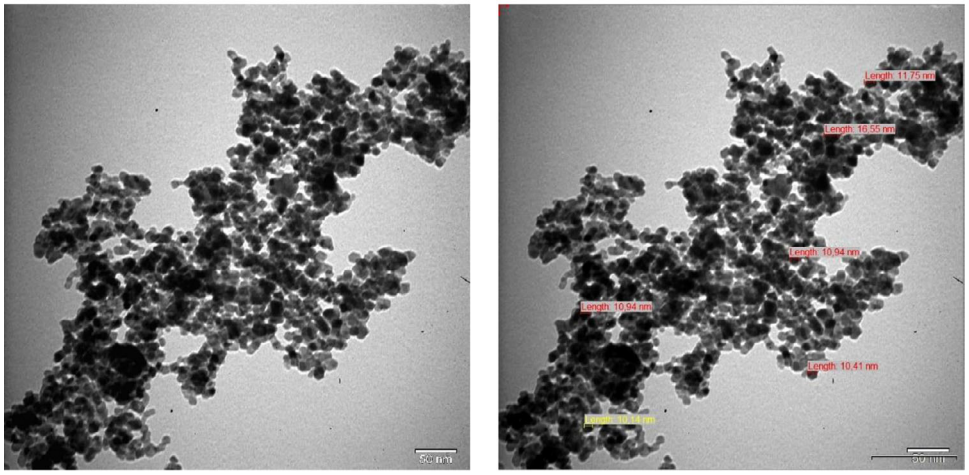

(B)

FIGURE 4 Continued

nitrogen physisorption isotherms at 77 K. Surface areas were defined by the BET techniques. Figure 5 represents the N_2 adsorption–desorption isotherm of the as-synthesized SnO_2 nanoparticles. This isotherm provides insights into the adsorption–desorption process occurring on the surface of the nanoparticles and indicates the pore structure of the adsorbent. Applied Chemistry (IUPAC), the as-prepared SnO_2 nanoparticles exhibit an isotherm of Type IV and display a mesoporous nature with H_3 hysteresis.[37]

Pore size distribution curves of synthesized SnO_2 samples were obtained using Barrett–Joyner–Halenda (BJH) techniques. Figure 6 indicates the relationship between the dV/dw pore volume and pore width. SnO_2, Ag–SnO_2, Pt/SnO_2, and Pt–Ag/SnO_2 samples had one peak in the pore width range of about 17, 16, 13, and 12.5 nm, respectively. Isotherm of all the samples resembled the type IV (IUPAC) isotherm and it signified that the materials were mesoporous.

One of the main factors that increase the photocatalytic activities of a material is the specific surface area and pore size distribution.[35] The plot of the BET function versus relative pressure is shown in Figure 7. The solid line seen here shows the characteristic properties of mesoporous solids.

Photocatalysts in the form of low-dimensional nanostructures have important advantages such as high surface area for redox reactions, fast electron and mass transfer, and high stability. It has been reported by Sathishkumar et al. that SnO_2 nanorods synthesized with large specific surface areas show good photocatalytic degradation performance.[38]

The BET surface areas of the as-prepared pure and doped SnO_2 nanoparticle are summarized in Table 3. It has been observed that Ag/SnO_2 nanopowder, which has the smallest particle size, also has the highest surface area value. When these results were examined together with the particle size results, it was seen that there was an inverse relationship between surface area and

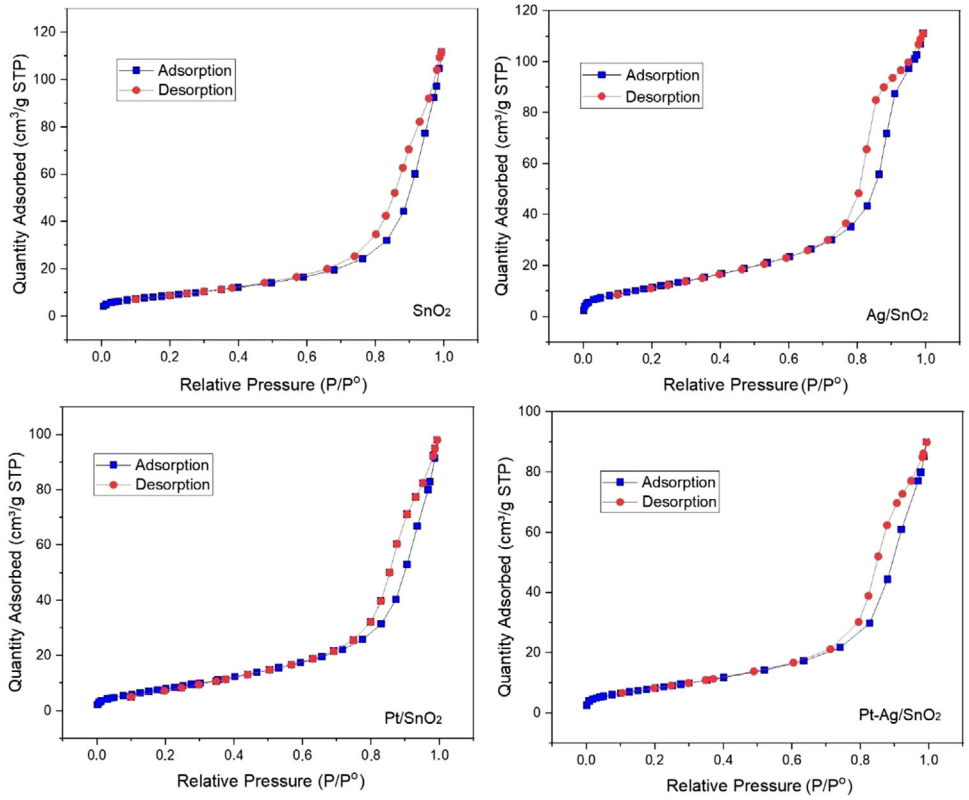

FIGURE 5 BET adsorption–desorption isotherm graph of the SnO_2 nanoparticles.

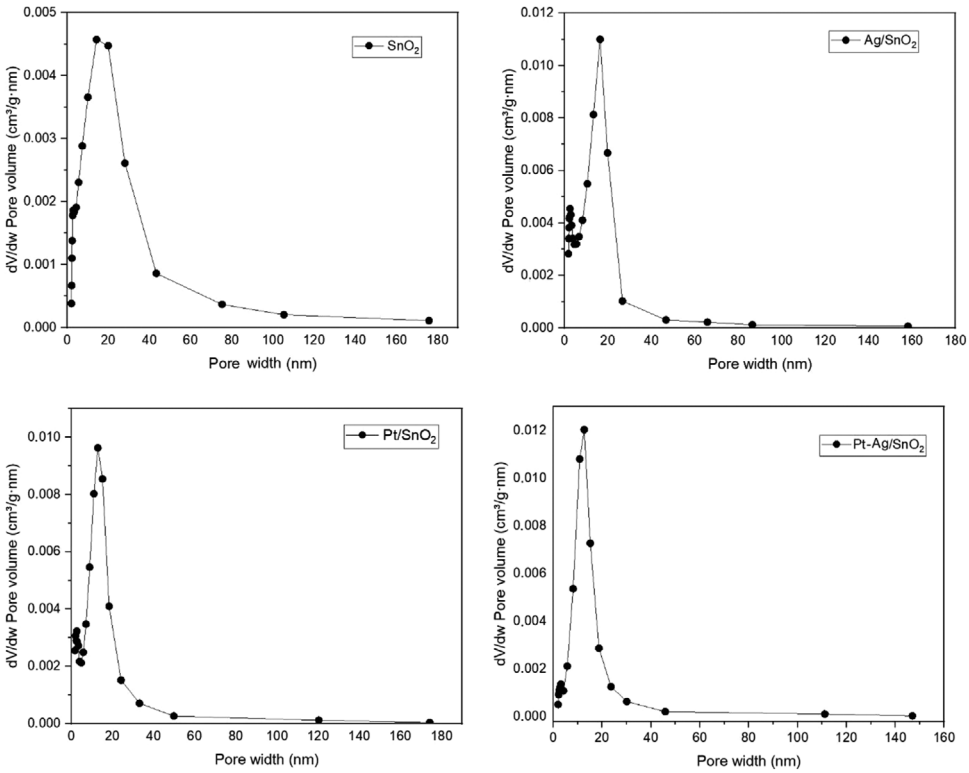

FIGURE 6 *dV*/*dw* pore volume and pore width computed by the BJH adsorption model.

TABLE 3 Physical properties of SnO_2 nanoparticles (surface areas, pore volumes, and average pore diameters).

Samples	BET surface area ($m^2\ g^{-1}$)	Single-point surface area at p/p^o ($m^2\ g^{-1}$)	Horvath–Kawazoe maximum pore volume ($cm^3\ g^{-1}$)	Pore size (nm)	Sample density ($g\ cm^{-3}$)	Nanoparticle size (nm)
SnO_2	33.02	31.66	.013021	15.2	1.0	181.70
Ag/SnO_2	46.22	42.09	.016680	13.03	1.0	129.8
Pt/SnO_2	34.03	29.88	.011503	13.37	1.0	176.29
$Pt–Ag/SnO_2$	32.20	29.93	.012068	13.71	1.0	186.32

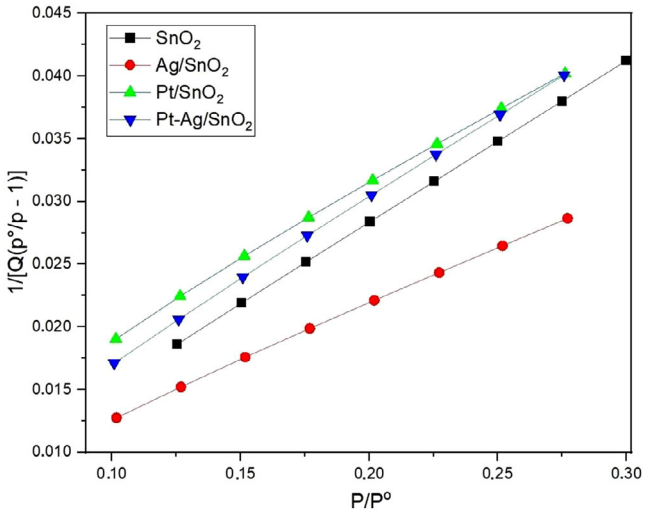

FIGURE 7 The plot of BET function vs. relative pressure.

nanoparticle size.[39] Additionally, it was determined that the SnO_2 surface had the most porous structure among the four analyzed samples. These results indicated that doped SnO_2 nanoparticles will improve photocatalytic properties with smaller particle sizes and larger surface areas.[40]

It was stated by Mao et al. that the adsorption capacity of dye molecules is related to their surface area and pore volume. It has been stated that ultra-small SnO_2 nanoparticles not only produce smaller pores but also expand the surface area of the composite. It has been reported that the addition of SnO_2 nanoparticles will cause the surface of TiO_2 films to be rougher, which will benefit the higher loading of dye molecules.[41]

The characteristic properties of SnO_2 nanoparticles synthesized with different combinations affected the specific surface area. In other words, it turns out that the specific surface area of the SnO_2 nanoparticle increases as the average particle size decreases. The observed high BET surface area for the Ag/SnO_2 nanoparticles is due to its lower particle size (129.8 nm) than pure SnO_2 (181.70 nm), Pt/SnO_2 (176.29 nm), and $Pt–Ag/SnO_2$ (186.32 nm) nanoparticles. The obtained results verify the relationship between surface areas and particle size of nanomaterials. These outcomes indicated that the physical and electrical properties of Ag/SnO_2 nanoparticles with lower particle size and higher surface area improved.[42]

3.3.2 | Particle size analysis

Figure 8 displays the size distribution of SnO_2 nanoparticles synthesized in different compositions. While the average particle size of the pure SnO_2 size was 222 nm, other doped Ag/SnO_2, Pt/SnO_2, and $Pt–Ag/SnO_2$ samples were 84, 121, and 115 nm, respectively. These results are in agreement with XRD, BET, and TEM analyses. As a result, doping processes led to particle size reductions.

3.4 | Optical properties

3.4.1 | UV—visible optical spectroscopy and band gap determination

The optical features of the synthesized SnO_2 nanoparticles were examined by UV–vis spectrophotometer. For this, the wavelength range from 200 to 800 nm was preferred. Figure 9 shows the obtained absorption spectrum of the synthesized SnO_2 nanoparticles. The first absorption maxima (λ_{max}) of the synthesized SnO_2, Ag/SnO_2, Pt/SnO_2, and $Pt–Ag/SnO_2$ nanoparticles were observed as 242.5, 267, 272.5, and 277 nm, respectively. The synthesized SnO_2 nanoparticles displayed a consistent increase between 800–400 nm. This trend demonstrated that there was no absorption in the visible region which is typical for wide band gap semiconductors.[43]

Optical band gap energy is given in Equation (4) and calculations were made using the Tauc relation.[44]

$$(\alpha h\upsilon) = A\left(h\upsilon - E_g\right)^{\frac{n}{2}}. \quad (4)$$

In this equation, 'α' is the optical absorption coefficient, 'h' is Planck's constant, 'A' is a constant, 'ν' is the frequency of the incident photon, '$h\nu$' is the energy of the incident photon, and 'E_g' is the energy of the optical band gap. The

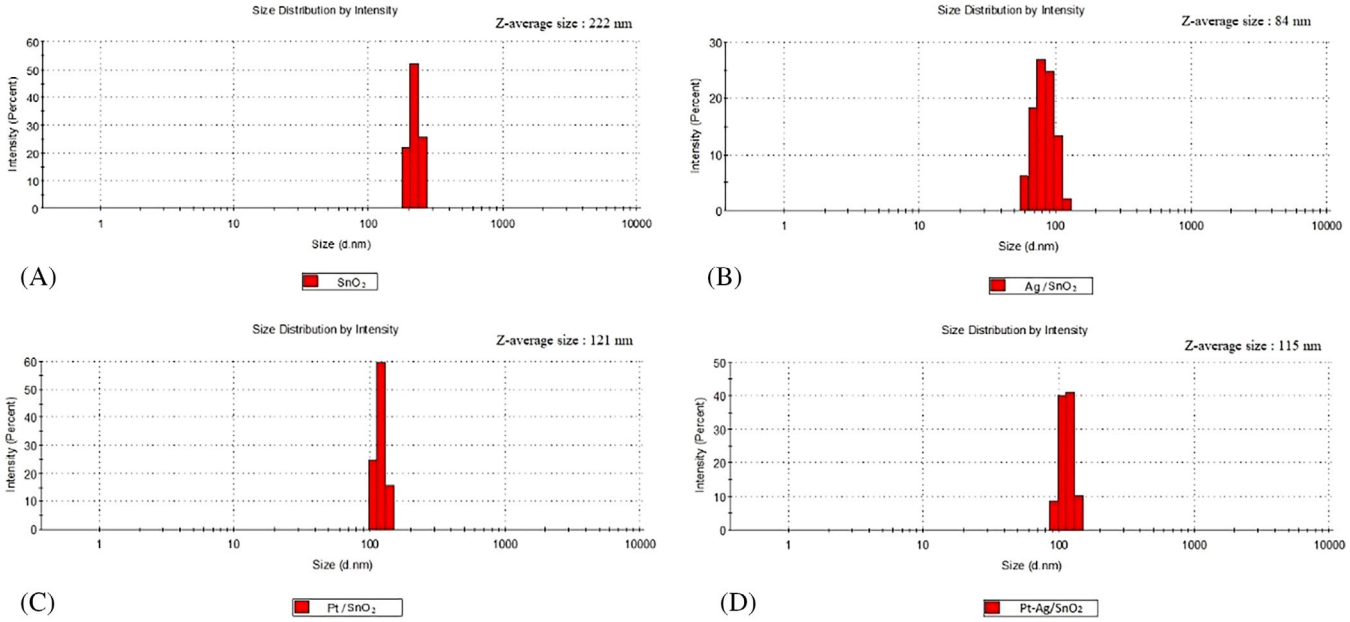

FIGURE 8 Particle size distribution of SnO_2 nanoparticles synthesized in different combinations.

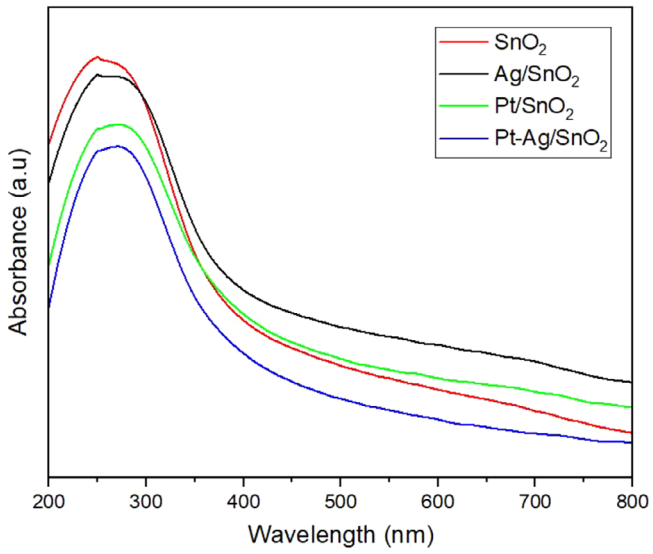

FIGURE 9 Absorbance spectrum of SnO_2 nanopowders.

exponent "n" is 1/2 for the direct and 2 for the indirect allowed transitions. The plot $(\alpha h\nu)^2$ versus $(h\nu)$ is occurred from it.[24]

In the Tauc plot graph, the linear part of the curve is extrapolated to $(\alpha h\nu)^2 = 0$. The direct and indirect band gap of the synthesized SnO_2 nanoparticles is extracted, as shown in Figure 10.

Band gap values are calculated by extrapolating the linear part of the curve obtained between $(\alpha h\nu)^2$ and $h\nu$. From the graphs drawn for SnO_2, Ag/SnO_2, Pt/SnO_2, and $Ag–Pt/SnO_2$ samples, band gap values were determined for each sample, and the relevant graph is given in Figure 11. According to the results obtained, the band gap observed in the pure SnO_2 sample was measured as 3.37 eV. Band gap values in doped samples (Pt/SnO_2, Ag/SnO_2, and $Pt–Ag/SnO_2$) were observed as 3.3, 3.09, and 3.15 eV, respectively. Therefore, the lowest band gap value was obtained from the Ag/SnO_2 sample. This decrease in the band gap is ascribed to the synergistic effect of the hybriding of the doped Ag metals with Sn. This causes a reduction in the conduction band minimum and an increment in the valence band maximum in the SnO_2 band structure.[19] In conclusion, the redshift in the energy gap and the appearance of a weak absorption shoulder in Ag-doped SnO_2 nanoparticles is due to charge transfer between SnO_2 and Ag atoms.[45,46] In general, doped SnO_2 samples have lower band gap values compared to the pure SnO_2 nanoparticular (Figure 11). This situation expresses that the doped metals doped the SnO_2 not only surface but also in the lattice of SnO_2.[43]

These conclusions are consistent with studies reported in the literature. They synthesized SnO_2 doped with Zn at different molar ratios (1%, 2%, 3%, and 4%). With increasing Zn^{2+} concentration, changes in the optical band gap were observed. While the optical band gap energy obtained for undoped SnO_2 was 3.68 eV, the band gap decreased to 3.41 eV with the increase of the Zn doping content in SnO_2 nanostructures. The reason for the decrease in the band gap is attributed to the formation of new energy levels between the conduction band and the valence band due to Zn substitution.[47]

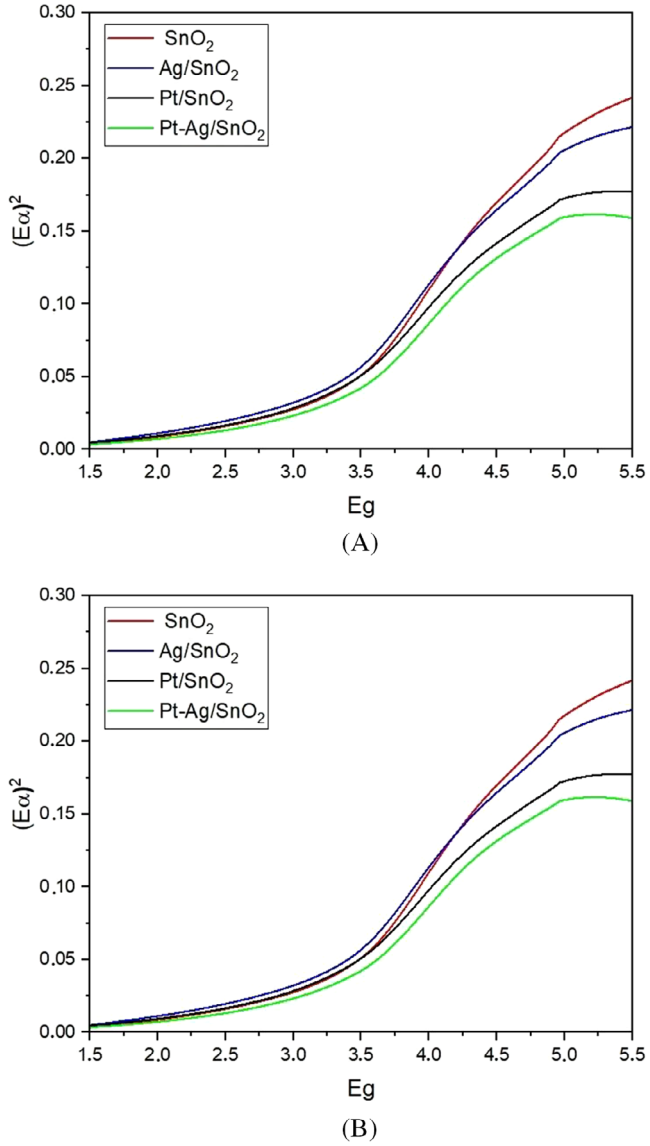

FIGURE 10 Tauc plot analysis indicates the (a) direct and (b) indirect band-gap transitions for synthesized SnO_2 nanoparticles.

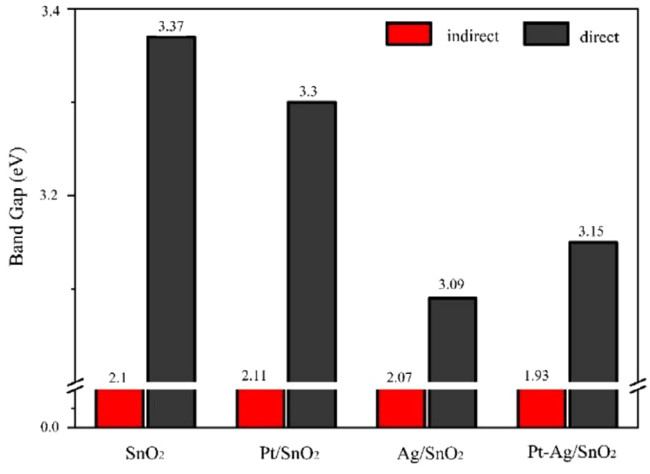

FIGURE 11 Direct and indirect optical band gaps of synthesized SnO_2 nanoparticles.

4 | CONCLUSIONS

In the study, doped SnO_2 samples were successfully synthesized by the sol–gel technique. It was determined by XRD patterns that the rutile phase nanoparticles had a tetragonal structure. The results showed that the crystal size was inversely proportional to the microstrain and dislocation density. Accordingly, while the average crystal size of the nanoparticles increased with Pt doping, it decreased especially with Ag doping and Pt–Ag co-doping. Therefore, the smallest average crystal size was acquired from the Ag-doped SnO_2 and Pt–Ag co-doped SnO_2 nanoparticle samples. These variations in particle size were also supported by the SEM and TEM analysis. These differences in the average crystallite sizes of the synthesized SnO_2 samples also led to a change in the band gap. Since SnO_2 is a compound with a complex electronic structure, its band gap decreased with doping. Pore width and dV/dw pore volume were computed by the BJH-adsorption. It has been determined that the pore width decreases with doping processes. While the maximum BET surface area was obtained with Ag doping, no significant change was observed in other dopings. Particle size analysis showed that the particle size decreased with doping processes, and the lowest particle size was obtained for the Ag/SnO_2 sample. It was confirmed that the synthesized samples were nanosized by XRD, SEM/EDX, TEM, BET, and particle size analyses. The small crystal size of the synthesized doped SnO_2 nanoparticles and high purity make them an ideal nominee as photoanode material in DSSC applications. These results are compatible with the literature and are promising for photoanode materials used in semiconductor technology, especially in DSSCs. Generally, the incorporation of metal ions into the SnO_2 nanostructure results in lower band gap values. This results in increased visible light absorption and therefore facilitates higher photocurrent.[48–50] The Ag/SnO_2 sample displays an important change in the band gap value of SnO_2 from 3.37 to 3.09 eV, allowing it to respond in the visible region. This decrease in the band gap is fatigued to the synergistic effect of hybriding of Pt and Ag species with Sn. Thus, localized defect levels are produced just above the valence band maximum of SnO_2. The combined effect of both the hybriding events results in a decrease in the band gap energy and development in the redshift.[6,51] These results show that Ag mono-doping and Pt/Ag co-doping shift band gap energies of SnO_2 to the longer wavelength side.[6] Moreover, metal doping like Ag in SnO_2 ensures higher surface area, stability, higher dye absorption, and retarded charge carrier recombination. Accordingly, Ag doping and Pt–Ag doping combination of metals can produce highly stable and efficient DSSCs.[43]

For this reason, it can be used as a convenient alternative nanomaterial for DSSC photoanode applications and photocatalysis processes.[20] This research, addressing the structural, morphological, and optical aspects of pure and Ag–Pt doped/co-doped SnO_2 nanoparticles, goal to convey useful information to the growing field of nanomaterials. The findings offered herein are expected to guide the optimization of SnO_2-based materials for DSSC applications.[10]

ACKNOWLEDGMENTS

The authors have nothing to report.

REFERENCES

1. Reddy CV, Babu B, Vattikuti SP, Ravikumar RVSSN, Shim J. Structural and optical properties of vanadium doped SnO_2 nanoparticles with high photocatalytic activities. J Lumin. 2016;179:26–34. https://doi.org/10.1016/j.jlumin.2016.06.036
2. Raju MJS, Bhattacharya SS. Structural and optical properties of Sb doped SnO_2 nanopowders synthesized by nebulized spray pyrolysis. Mater Today Proc. 2018;5:10097–103. https://doi.org/10.1016/j.matpr.2017.11.005
3. Muchuweni E, Martincigh BS, Nyamori VO. Recent advances in graphene-based materials for dye-sensitized solar cell fabrication. RSC Adv. 2020;10:44453–69. https://doi.org/10.1039/D0RA08851J
4. Dhonde M, Sahu K, Das M, Yadav A, Ghosh P, Murty VVS. Recent advancements in dye-sensitized solar cells; from photoelectrode to counter electrode. J Electrochem Soc. 2022;169(6):066507. https://doi.org/10.1149/1945-7111/ac741f
5. Sharma K, Sharma V, Sharma SS. Dye-sensitized solar cells: fundamentals and current status. Nanoscale Res Lett. 2018;13:1–46. https://doi.org/10.1186/s11671-018-2760-6
6. Gupta A, Sahu K, Dhonde M, Murty VVS. Novel synergistic combination of Cu/S co-doped TiO_2 nanoparticles incorporated as photoanode in dye sensitized solar cell. Sol Energy. 2020;203:296–303. https://doi.org/10.1016/j.solener.2020.04.043
7. Vasanthapriya R, Neelakandeswari N, Rajasekaran N, Uthayarani K, Chitra M. Synthesis and characterization of SnO_2 nanostructures for dye-sensitized solar cells. Mater Lett. 2018;220:218–21. https://doi.org/10.1016/j.matlet.2018.02.118
8. Dhonde M, Sahu K, Murty VVS. Cu-doped TiO_2 nanoparticles/graphene composites for efficient dye-sensitized solar cells. Sol Energy. 2021;220:418–24. https://doi.org/10.1016/j.solener.2021.03.072
9. Saleem SA, Yadav SC, Srivastava A, Kanwade A, Tiwari MK, Rajore SM, et al. The dynamic synergy of tin in electron transfer layer and absorber layer for advancing perovskite solar cells: a comprehensive review. Energy Adv. 2024;3:1505–1552. https://doi.org/10.1039/D4YA00204K
10. Prajapat K, Mahajan U, Dhonde M, Sahu K, Shirage PM. Synthesis and characterization of TiO_2 nanoparticles: unraveling the influence of copper doping on structural, surface morphology, and optical properties. Chem Phys Impact. 2024;8:100607. https://doi.org/10.1016/j.chphi.2024.100607
11. Xu B, Chen Z, Li S. Aluminum-doped SnO_2 hollow microspheres as photoanode materials for dye-sensitized solar cells. Int J Photoenergy. 2016;1:3129896. https://doi.org/10.1155/2016/3129896
12. Hu Y, Li L, Xu C, Yang P. Study of high metal doped SnO_2 for photovoltaic devices. Mater Today Commun. 2021;27:102148. https://doi.org/10.1016/j.mtcomm.2021.102148
13. Ahmad T, Ansari MZ. Structural and optical characteristics of Sb doped SnO_2 nanoparticles and their boosted photocatalytic activity under visible light irradiation. Ceram Int. 2023;49:35740–56. https://doi.org/10.1016/j.ceramint.2023.08.253
14. Siregar N, Motlan, Panggabean JH, Sirait M, Rajagukguk J, Gultom NS, et al. Fabrication of dye-sensitized solar cells (DSSC) using Mg-doped ZnO as photoanode and extract of rose myrtle (*Rhodomyrtus tomentosa*) as natural dye. Int J Photoenergy. 2021;1:403369. https://doi.org/10.1155/2021/4033692
15. Li X, Yu Q, Yu C, Huang Y, Li R, Wang J, et al. Zinc-doped SnO_2 nanocrystals as photoanode materials for highly efficient dye-sensitized solar cells. J Mater Chem A. 2015;3:8076–82. https://doi.org/10.1039/C5TA01176K
16. Panneer NK, Venkatraman C, Bachan N, Wilson JJ, Edwin MA, Jesudasan AR, et al. Ecofriendly sol-gel-derived dye-sensitized solar cells with aluminium-doped tin oxide photoanode. Environ Sci Pollut Res. 2023;30(21):60524–37. https://doi.org/10.1007/s11356-023-26733-8
17. Khan D, Rehman A, Rafiq MZ, Khan AM, Ali M. Improving the optical properties of SnO_2 nanoparticles through Ni doping by sol–gel technique. Curr Res Green Sustain Chem. 2021;4:100079. https://doi.org/10.1016/j.crgsc.2021.100079
18. Lachore WL, Andoshe DM, Hone FG, Mekonnen MA. Structural, optical and electrical properties of copper (Cu) and [nickel (Ni), copper]: co-doped SnO_2 nanoparticles prepared by sol–gel method. Appl Phys A. 2022;128(6):515. https://doi.org/10.1007/s00339-022-05655-1
19. Dhonde M, Sahu Dhonde K, Purohit K, Murty VVS. Facile synthesis of Cu/N co-doped TiO_2 nanoparticles and their optical and electrical properties. Indian J Phys. 2019;93(1):27–32. https://doi.org/10.1007/s12648-018-1275-4
20. Mahajan U, Srivastava A, Dhonde M, Sahu K, Ghosh P, Shirage PM. Zinc-modified barium stannate microrods: investigating structural, morphological, and optical features. Chem Phys Impact. 2024;8:100622. https://doi.org/10.1016/j.chphi.2024.100622
21. Aydın Ünal F, Ünal M, Ataşer T, Özçelik S. Synthesis, characterization, photocatalytic application of Gd/K co-doped ZnO. Int J Appl Ceram Technol. 2024;21(1):349–57. https://doi.org/10.1111/ijac.14517
22. Navas D, Fuentes S, Castro-Alvarez A, Chavez-Angel E. Review on sol–gel synthesis of perovskite and oxide nanomaterials. Gels. 2021;7:275. https://doi.org/10.3390/gels7040275
23. Sun C, Yang J, Xu M, Cui Y, Ren W, Zhang J, et al. Recent intensification strategies of SnO_2-based photocatalysts: a review. Chem Eng J. 2022;427:131564. https://doi.org/10.1016/j.cej.2021.131564
24. Naz S, Javid I, Konwar S, Surana K, Singh PK, Sahni M, et al. A simple low-cost method for synthesis of SnO_2 nanoparticles and its characterization. SN Appl Sci. 2020;2:1–8. https://doi.org/10.1007/s42452-020-2812-2
25. Guo L, Liang H, An D, Yang H. One-step hydrothermal synthesis of uniform Ag-doped SnO_2 nanoparticles for highly sensitive ethanol sensing. Physica E. 2023;151:115717. https://doi.org/10.1016/j.physe.2023.115717
26. Setiadji S, Ulfah R, Wahyuni IR. Synthesis of SnO_2 using hydrothermal method and its application as catalyst in

esterification of oleic acid. Walisongo J Chem. 2021;4(2):90–96. https://doi.org/10.21580/wjc.v4i2.7911
27. Quan W, Hu X, Min X, Qiu J, Tian R, Ji P, et al. A highly sensitive and selective ppb-level acetone sensor based on a Pt-doped 3D porous SnO_2 hierarchical structure. Sensors. 2020;20:1150. https://doi.org/10.3390/s20041150
28. Sinha SN, Yadav H, Godara S, Joseph AJ, Kumar B. Ferroelectric Gd-doped ZnO nanostructures: enhanced dielectric, ferroelectric and piezoelectric properties. Mater Chem Phys. 2017;202:56–64. https://doi.org/10.1016/j.matchemphys.2017.08.067
29. Madhavi JJSAS. Comparison of average crystallite size by X-ray peak broadening and Williamson–Hall and size–strain plots for VO^{2+} doped ZnS/CdS composite nanopowde. SN Appl Sci. 2019;1:1509. https://doi.org/10.1007/s42452-019-1291-9
30. Yaacoub Bouderbala I, Guessoum A, Rabhi S, Bouhlassa O, Bouras IE. Optical band diagram, Urbach energy tails associated with photoluminescence emission in defected ZnO thin films deposited by sol–gel process dip-coating: effect of precursor concentration. Appl Phys A: Mater Sci Process. 2024;130:1–19. https://doi.org/10.1007/s00339-024-07366-1
31. Shamhari NM, Wee BS, Chin SF, Kok KY. Synthesis and characterization of zinc oxide nanoparticles with small particle size distribution. Acta Chim Slov. 2018;65:578–85. https://doi.org/10.17344/acsi.2018.4213
32. Turan E, Kul M, Akın S. Structural and optical investigation of spray-deposited SnO_2 thin films. J Mater Sci: Mater Electron. 2022;33:15689–703. https://doi.org/10.1007/s10854-022-08472-7
33. Gubicza J, Szépvölgyi J, Mohai I, Zsoldos L, Ungár T. Particle size distribution and dislocation density determined by high-resolution X-ray diffraction in nanocrystalline silicon nitride powders. Mater Sci Eng A. 2000;280:263–69. https://doi.org/10.1016/S0921-5093(99)00702-9
34. Mangaiyarkkarasi J, Meenakumari V, Thenmozhi N. Microstructural and morphological insight of wide band gap SnO_2 towards gas sensor applications. Sādhanā. 2023;48:86. https://doi.org/10.1007/s12046-023-02138-8
35. Guo L, Liang H, An D, Yang H. One-step hydrothermal synthesis of uniform Ag-doped SnO_2 nanoparticles for highly sensitive ethanol sensing. Physica E. 2023;151:115717. https://doi.org/10.1016/j.physe.2023.115717
36. Sery AA, Mohamed WA, Hammad FF, Khalil MM, Farag HK. Synthesis of pure and doped SnO_2 and NiO nanoparticles and evaluation of their photocatalytic activity. Mater Chem Phys. 2022;275:125190. https://doi.org/10.1016/j.matchemphys.2021.125190
37. Sudha Periathai R, Pon Venkatesh R, Abarna S, Prithivikumaran N. Treatment of water pollution system using SnO_2 nanoparticles synthesized by sol–gel process. Appl Nanosci. 2024;14:135–47. https://doi.org/10.1007/s13204-023-02965-5
38. Sathishkumar S, Parthibavarman M, Sharmila V, Karthik M. A facile and one step synthesis of large surface area SnO_2 nanorods and its photocatalytic activity. J Mater Sci: Mater Electron. 2017;28:8192–96. https://doi.org/10.1007/s10854-017-6529-y
39. Li Y, Li L, Zhang R, Ying Z, Zhou Y, Wu W, et al. Effect of SnO_2 particle size on gas-sensing performance for ppb-level NO_2 at room temperature under UV light. J Mater Sci: Mater Electron. 2024;35(3):236. https://doi.org/10.1007/s10854-023-11876-8
40. Manimaran M, Muthuvel A, Said NM. Microwave-assisted green synthesis of SnO_2 nanoparticles and their photocatalytic degradation and antibacterial activities. Nanotechnol Environ Eng. 2023;8:413–23. https://doi.org/10.1007/s41204-022-00297-3
41. Mao X, Zhou R, Zhang S, Ding L, Wan L, Qin S, et al. High efficiency dye-sensitized solar cells constructed with composites of TiO_2 and the hot-bubbling synthesized ultra-small SnO_2 nanocrystals. Sci Rep. 2016;6(1):19390. https://doi.org/10.1038/srep19390
42. Suresh KC, Surendhiran S, Manoj Kumar P, Ranjth Kumar E, Khadar YS, Balamurugan A. Green synthesis of SnO_2 nanoparticles using Delonix elata leaf extract: evaluation of its structural, optical, morphological and photocatalytic properties. SN Appl Sci. 2020;2:1–13. https://doi.org/10.1007/s42452-020-03534-z
43. Unal FA, Ok S, Unal M, Topal S, Cellat K, Şen F. Synthesis, characterization, and application of transition metals (Ni, Zr, and Fe) doped TiO_2 photoelectrodes for dye-sensitized solar cells. J Mol Liq. 2020;299:112177. https://doi.org/10.1016/j.molliq.2019.112177
44. Salehi A, Ghodsi FE, Mazloom J, Ebrahimi-Koodehi S. Tuning of optical bandgap, conductivity parameters, and PL emissions of SnO_2:Ni thin films under Ar, N_2, and O_2 annealing. Appl Phys A: Mater Sci Process. 2018;124:1–6. https://doi.org/10.1007/s00339-018-2087-2
45. Vignesh K, Hariharan R, Rajarajan M, Suganthi A. Photocatalytic performance of Ag-doped SnO_2 nanoparticles modified with curcumin. Solid State Sci. 2013;21:91–99. https://doi.org/10.1016/j.solidstatesciences.2013.04.017
46. Suriya P, Prabhu M, Jagannathan K. Effect of Ag doping on structural, optical, complex impedance and photovoltaic properties of SnO_2 nanoparticles prepared by co-precipitation method for dye sensitized solar cell application. Optik. 2022;260:168971. https://doi.org/10.1016/j.ijleo.2022.168971
47. Habte AG, Hone FG, Dejene FB. Zn doping effect on the properties of SnO_2 nanostructure by co-precipitation technique. Appl Phys A. 2019;125(6):402. https://doi.org/10.1007/s00339-019-2695-5
48. Dhonde KS, Dhonde M, Murty VVS. Novel synergistic combination of Al/N Co-doped TiO_2 nanoparticles for highly efficient dye-sensitized solar cells. Sol Energy. 2018;173:551–57. https://doi.org/10.1016/j.solener.2018.07.091
49. Dhonde M, Sahu K, Murty VVS, Nemala SS, Bhargava P. Surface plasmon resonance effect of Cu nanoparticles in a dye sensitized solar cell. Electrochim Acta. 2017;249:89–95. https://doi.org/10.1016/j.electacta.2017.07.187
50. Neetu, Maurya IC, Gupta AK, Srivastava P, Bahadur L. Extensive enhancement in power conversion efficiency of dye-sensitized solar cell by using Al-doped TiO_2 photoanode. J Solid State Electrochem. 2017;21:1229–41. https://doi.org/10.1007/s10008-016-3478-y
51. Cravanzola S, Cesano F, Gaziano F, Scarano D. Sulfur-doped TiO_2: structure and surface properties. Catalysts. 2017;7(7):214. https://doi.org/10.3390/catal7070214

How to cite this article: Aydın Ünal F. Synthesis and characterization of the doped/co-doped SnO_2 nanoparticles by the sol–gel method. Int J Appl Ceram Technol. 2025;22:e14916. https://doi.org/10.1111/ijac.14916